The Discharge Coefficient of a Planar Submerged Slit-Jet

S. K. Ali
Visteon Corporation,
Rawsonville Plant,
10300 Textile Road,
Ypsilanti, MI 48197
e-mail: sali5@visteon.com

J. F. Foss
Department of Mechanical Engineering,
Michigan State University,
East Lansing, MI 48824
e-mail: foss@egr.msu.edu

The discharge coefficient, C_D, of a planar, submerged slit-jet has been determined experimentally over a relatively wide range of Reynolds number values: $Re=100-6500$, where the slit width (w) and the average streamwise velocity ($\langle U\rangle$) at the exit plane are used to define the Reynolds number. The C_D values exhibit a strong dependence on Re for $Re<800$. For $Re>3000$, C_D achieves an apparent asymptotic value of 0.687 for the present nozzle design. This value is about 12% higher than the potential flow value. In contrast, the velocity distribution along the centerline was in excellent agreement with that of the potential flow solution. The experimental techniques that were used to evaluate the $C_D(Re)$ values, their numerical values, the corresponding uncertainties, and the possible influence of the geometrical design of the nozzle on the results are presented.
[DOI: 10.1115/1.1593712]

Introduction

The discharge coefficient, C_D, of a nozzle or other constriction is a characteristic of practical significance. For low-subsonic flows, C_D depends both on the flow-field geometry and flow Reynolds number. Blevins [1] provides representative values. The discharge coefficient of a planar, or quasi-two-dimensional, submerged slit-jet is considered in the present communication. A two-dimensional slit-jet, which can be easily simulated using a large aspect ratio: $B_N/w \gg 1$, opening in the wall of a plenum, has been analyzed using potential flow methods; see Birkhoff and Zarantonello [2] and Vallentine [3]. The analytical value of the discharge coefficient of a slit-jet, which delivers an inviscid fluid from an ''infinite'' plenum, is 0.611. The effect of a finite plenum width (H), for a two-dimensional orifice, has been analytically evaluated by Ali [4] using potential flow methods. These calculations show that $C_D(H/w \geqslant 10)$ is negligibly different from $C_D(H/w=\infty)$. The minimum value of H/w for the present study was selected as 18 which removes the influence of this parameter on the C_D value.

The development of a vena-contracta, with the corresponding contraction of the separating streamlines and the acceleration of the centerline fluid elements to the maximum velocity magnitude U_0, is a distinctive feature of both circular and planar (as studied herein) sharp-edged orifices. For the flow of an inviscid fluid through a slit jet, the separating streamlines continue to contract, and the vena-contracta is asymptotically approached. However, for a physical submerged jet, the vena-contracta has been found to occur at about one slit-width downstream from the exit plane; see Ali [4]. Physical jets also exhibit natural instabilities which result in the formation of symmetric and ''two-dimensional'' vortices along the shear layers. These vortex motions have been studied by Beavers and Wilson [5], Clark and Kit [6], Foss and Korschelt [7], and Ali [4].

For a slit-jet, the discharge coefficient C_D is defined as

$$C_D=\frac{\int_A \mathbf{V}(0,y,z)\cdot \mathbf{i}dA}{U_0 A_j}, \tag{1}$$

where $\mathbf{V}(0,y,z)$ is the time-mean velocity vector at the exit plane of the jet, $\mathbf{i}$ is the unit vector in the streamwise (x) direction, U_0 is the maximum velocity on the centerline ($\overline{u}(x,0)\rightarrow U_0$ for $x\approx w$ and for sufficiently large Re values), and A_j is the area of the orifice given by the product: (wxB_N), where B_N denotes the breadth of the nozzle. In terms of the spatial average velocity, $\langle U\rangle$, which is defined as

$$\langle U\rangle=\frac{1}{A_j}\int_A \mathbf{V}(0,y,z)\cdot \mathbf{i}dA, \tag{2}$$

the discharge coefficient becomes

$$C_D=\frac{\langle U\rangle}{U_0}. \tag{3}$$

The measurement techniques to determine $\langle U\rangle$ and U_0 are described in the following section.

The purpose of this paper is to

i. present the experimentally determined values of the discharge coefficient C_D of the present submerged slit-jet over the Reynolds number range: $100\leqslant \mathrm{Re}\leqslant 6500$,
ii. compare the experimental results with the potential flow solution of the slit-jet flow field emanating from a finite width (H) plenum as shown in Fig. 1,
iii. discuss the influence of the nozzle plate geometry—as expressed by its thickness (t_N) and the inclination angle (α_N) of the relieved surface (see Fig. 1)—on the value of C_D, and
iv. present an explanation for the differences (as well as the elements of agreement) between the experimental results and the corresponding quantities in the potential flow solution.

Experimental Configuration

Figure 1 is a schematic representation of the flow facility that was used in this investigation. It was designed with $H/w>10$, so that the influence of the ''outer'' side walls on the development of the jet is minimal. Water or a water-sugar mixture were used as the working liquids in this finite duration, gravity driven, ''steady'' flow facility. (This unique experimental facility has been fully described by Ali and Foss [8]). As shown in Fig. 1, the present flow facility is comprised of two major units: (i) a glass tank (A), and (ii) a clear plastic structure called the nozzle housing (NH) which is given the code description ''C'' in Fig. 1. The two nozzle plates with beveled edges are supported at right angles to the jet-axis by the NH; the nozzle plates form the planar slit-jet. The tank is filled with a working liquid such that its level is above the nozzle plates under the conditions of static equilibrium. The liquid-filled space above the nozzle plates is designated ''the plenum;'' the space below is called ''the receiver.'' The portion of the enclosed space above the nozzle plates, that is not liquid filled, is

Contributed by the Fluids Engineering Division for publication in the JOURNAL OF FLUIDS ENGINEERING. Manuscript received by the Fluids Engineering Division June 19, 2000; revised manuscript received February 28, 2003. Associate Editors: B. Schiavello.

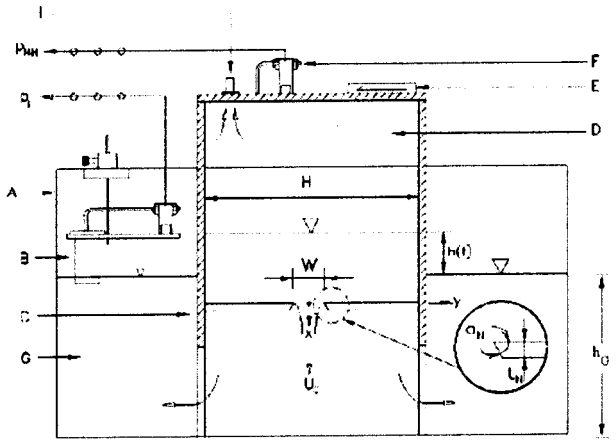

Fig. 1 Schematic representation of the operational features of the flow facility. A: 0.2 cubic meter (80 gal.) glass tank; B: volume flow sensor (VFS); C: nozzle housing (NH); D: low pressure cavity ($p_{NH}(t)$); E: bleed valve; F: pressure transducer; G: receiver; I: connection to vacuum tank. ——→ pointer, ——→ velocity (flow), -o-o-o-o- signal, ——v—— free surface

termed the ''low pressure cavity (*D*).'' The NH has partially open sides below the plane of the nozzle plates (see the outflow to the receiver in Fig. 1) and an air tight cover plate (above the nozzle plates) which supports a bleed valve (*E*). There are two additional openings in the cover plate: (i) a pressure tap connected to a pressure transducer (*F*), and (ii) a vacuum tank connection (*I*). The latter is used to lower the pressure in *D* thus raising the liquid head (h) in the NH. The slit-jet flow is caused by allowing atmospheric air to enter at a controlled rate through the bleed valve. This valve is operated by a computer controlled stepper motor to ensure a satisfactory approximation to a time steady exit flow from the plenum during the data acquisition period. Specifically, the pressure in *D* is linearly increased with respect to time in order to compensate for the linear decrease in the differential elevation, h, between the plenum and the receiver. In combination, the net effect is $dU_0/dt=0$ during the period of data acquisition.

Concurrent measurements were made over a wide range of Re (100–6500) to determine the two velocities, $\langle U\rangle$ and U_0. Specifically, a single channel laser Doppler velocimeter (LDV) was used to measure the time average velocity on the centerline, U_0, at $x/w\cong 2$. The spatial-average velocity $\langle U\rangle$ was determined by using a novel device, a volume flow sensor (VFS), as shown by ''*B*'' on the left-hand side of Fig. 1. The air, that is trapped in the inverted cup, is pressurized as the water level in the receiver tank is increased during the ''run time'' of the experiment. Since a precise relationship, as described in the next section, can be experimentally established between water level and the pressure in the inverted cup, and since the water level in the receiver increases slowly, the air pressure: $p_l(t)$, value from the cup provides a reliable measure of the time-dependent volume of fluid in the receiver and, hence, its time derivative that is equal to the discharge flow rate, $\int\int u(x=0,y,z,t)dydz$.

Ideally the nozzle plates should be very thin. However, for practical reasons of strength, the nozzle plates were fabricated using $t_N=12.7$ mm stock. The plates were beveled at an angle $\alpha_N=60$ deg with respect to the plane of the nozzle plates, see Fig. 1 for the definition of α_N. Two values were used for the width, w, of the slit-jet: 12.7 mm and 25.4 mm. Hence, the ratio t_N/w was 1 and 0.5, respectively. The aspect ratio, B_N/w, was equal to 21.7 and 10.8, respectively.

Evaluation of C_D

The companion paper, Ali and Foss [8], provides a detailed description of the flow control process that provides a steady-state slit-jet flow for an elapsed time that is sufficient to record statistically stationary centerline velocity $\overline{u}(x/w=2,0)=U_0$ and the jet exit average velocity $\langle U\rangle$. These values represent the flow behavior at a given Re and t_N/w.

The LDV measurements of $u(x/w=2,0,t)$ are averaged over the same time period, Δt, as that for $\langle U\rangle$ to yield U_0. In this manner, the $C_D(\mathrm{Re},t_N/w)$ values can be obtained as shown in Eq. (3). The evaluation of the $\langle U\rangle$ and the U_0 values, that are to be used in establishing $C_D=C_D(\mathrm{Re},t_N/w)$, are the essence of the present contribution. As such, considerable care will be taken in identifying the source of these values including the bases for their uncertainty estimates. These considerations are given in the following subsections.

Evaluation of U_0

A Thermo Systems Inc., 35 mW He-Ne LDV system (primitive by today's standards but adequate for the task at the time of its execution *and* for the required purpose of providing $u(x/w=2,0,t)$ as an accurately determined quantity) was used in this study. A counter-system (Model TSI 1980) was used to determine the Doppler shift frequency of the small particles that reliably follow the fluid velocity in this benign ($U_0\partial U_0/\partial x=0$) environment. The fixed volume of liquid in the glass tank identified by *A* in Fig. 1, made it a relatively simple matter to obtain a densely seeded environment; polyvinyltoluene particles with a mean diameter of 2μ were used to provide the scattering centers. Hence, the preset counter output frequency: 308 Hz was readily met with updated velocity values. For reference, at a Re value of 3000 and jet width $w=12.7$ mm, this sample rate nominally provides a measured velocity value each 0.77 mm or 0.06 w. For the same Re value and $w=25.4$ mm, the spacing is 0.38 mm or 0.015 w.

Individual $u(x,0,t)$ measurements are, in principle, subject to the LDV phenomenon of velocity bias (where high-speed fluid elements have a larger probability of being ''captured'' by the instrument); see, e.g., Adrian [9]. This effect is, of course, exacerbated if the velocity variation at a given location exhibits a ''wide'' probability density function (pdf) and if there are significant time delays between data samples. The above discussion shows that the latter effect is not a factor in these measurements. The measured intensities (Ali [4]) were of order $0.1(=\tilde{u}/U_0)$ at the $x/w=2$ measurement location. Hence, velocity bias effects in the present experiment will not influence the integrity of the U_0 measurements.

Evaluation of $\langle U\rangle$

A single device, the volume flow sensor (VFS), was used to determine $\langle U\rangle$ for the present experiments. The VFS takes advantage of two intrinsic attributes of this experiment: (i) the receiving reservoir (*G* of Fig. 1) is characterized by an area: A_r, that is $31\times A_j$ for $w=25.4$ mm (or, $62\times A_j$ for $w=12.7$ mm), and (ii) air, at low-pressure rise values, is incompressible. Hence, the VFS of Fig. 1, will remain void of liquid as the liquid level around it is raised in the experiment. The air pressure, however, will be increased in proportion to the increasing submerged depth, h_l, of the VFS. This correlation between the rise in the liquid level and the rise in the pressure in the inverted cup was used to calibrate the VFS. The calibration method is described below:

Consider that the nozzle opening is blocked for a condition where the initial water level: $h_o(1)$, in ''*G*'' is known. If a controlled amount of water (M_c) is added to the reservoir *G*, then the water level rise ($h_o(2)-h_o(1)$) can be correlated with the added water. The inverted cup of the VFS will be slightly submerged for the condition: $h_o=h_o(1)$. There will be a corresponding voltage ($E_p(1)$) from the pressure transducer. Following the addition of the water, the voltage increment

$$\Delta E_p(1)=[E_p(2)-E_p(1)] \tag{4a}$$

$$=C_p\rho g[h_o(2)-h_o(1)] \tag{4b}$$

Table 1 Estimates of errors in the width w, span B_N, and the area of the jet A_j for the two jets

w m	δw m	B_N m	δB_N m	A_j m^2	δA_j m^2
0.0127	4×10^{-5}	0.275	5×10^{-4}	3.4836×10^{-3}	3.4644×10^{-5}
0.0254	6×10^{-5}	0.275	5×10^{-4}	6.9946×10^{-3}	6.8416×10^{-5}

will be recorded as the output from the pressure transducer; here, C_p is the calibration constant for the pressure transducer. Hence, the first controlled mass of water: $M_c(1)$, will be proportional to the increment in E_p as

$$M_c(1)\sim\Delta E_p(1). \tag{4c}$$

This provides a calibration technique:

$$M_c\sim\Delta E_p. \tag{4d}$$

If the confining walls of the glass tank are vertical, then

$$\Delta E_p=C_m\rho A_r\Delta h_o. \tag{4e}$$

This calibration procedure included measurement of the density of water using a picnometer. For M_c, a top-loading weighing scale was used to measure water in amounts of 15 pounds (6.8 kg), or 30 pounds (13.6 kg) at a time to pour into the tank G. The height of the water in the four corners of G was measured using a steel rule, and the laboratory computer was used to digitize E_p. An average height, h_G, of the water in the tank was found for each addition of M_c. Using the measured density of the water, the volume of water poured, V_C, was determined from M_C for each case; V_C was then used to determine the area of the receiver $A_r(h_G)$ at each height h_G. The average value of A_r was found to be 0.2136 square meter with standard deviation equal to 0.0004 square meter or nominally 0.2% of the mean area.

A linear regression analysis between the measured voltage E_p and the average height h_G yielded

$$h_G=\beta_0+\beta_1E_p \tag{5}$$

where β_0 and β_1 are the coefficients of the linear regression. The estimates of β_0 and β_1 were 0.03255 mm and 25.2201 mm/volt, respectively, and the corresponding estimates of standard error were found to be 7.933E-3 mm and 3.572E-3 mm/volt.

In a given experiment, the voltage increase ΔE_p, corresponding to the pressure rise in the cup, was measured over a given time interval Δt, which is the same as the interval for which the centerline velocity data $u(x=2w,y=0,t)$ were acquired using the LDV system described above. Using $\Delta(E_p)/\Delta(t)$ in the calibration equation yielded the average rate of rise of water in the receiver V_r:

$$V_r=\Delta h_G/\Delta t=\beta_1\Delta E_p/\Delta t. \tag{6}$$

The use of the continuity equation to equate the outflow from the plenum to the receiver-inflow yielded the temporal/spatial average velocity of the jet $\langle U\rangle$, which is expressed as

$$\langle U\rangle=\beta_1\frac{A_r}{A_j}\frac{\Delta E_p}{\Delta t}. \tag{7}$$

Uncertainty Analysis

A conservative estimate of relative uncertainty in C_D, $\delta C_D/C_D$, can be obtained from the general error propagation formula:

$$\delta C_D/C_D=[(\delta\langle U\rangle/\langle U\rangle)^2+\delta(U_0/U_0)^2]^{1/2}, \tag{8}$$

where $\delta\langle U\rangle/\langle U\rangle$ and $\delta U_0/U_0$ are the relative uncertainties in the spatial/temporal average velocity and the maximum centerline velocity of the jet, respectively. It will be shown at the end of this section that the uncertainty in $\langle U\rangle$ is the dominant term and represents the uncertainty in C_D.

The relative uncertainty in $\langle U\rangle$: $\delta\langle U\rangle/\langle U\rangle$, was determined using the general error propagation formula applied to Eq. (7). It is expressed as

$$\frac{\delta\langle U\rangle}{\langle U\rangle}=\left[\left(\frac{\delta(\Delta E_p)}{\Delta E_p}\right)^2+\left(\frac{\delta(\Delta t)}{\Delta t}\right)^2+\left(\frac{\delta A_r}{A_r}\right)^2+\left(\frac{\delta A_j}{A_j}\right)^2+\left(\frac{\delta\beta_1}{\beta_1}\right)^2\right]^{1/2}. \tag{9}$$

The first term, of the five terms on the right-hand side of Eq. (10), is the largest. It depends upon the execution of the experiment at a given Re, and the characteristic of the pressure transducer used. For the present work, the first term was evaluated from the characteristic of the Validyne DP15-22 pressure transducer and the measured voltage difference ΔE_p in the cup for each experiment. More specifically, the estimate of error $\delta(\Delta E_p)$ was obtained from the linearity specification: 0.2% of the full scale of the pressure transducer; this translated to ±0.01016 volt. A conservative estimate: 0.0212 volt was used for $\delta(\Delta E_p)$, for evaluation.

The time: $\Delta t=13.3$ seconds, was used in all measurements for Re$<$4000. For higher Re values, Δt was reduced to shorter times of about eight seconds to accommodate the height of the inverted cup. Specifically, the larger flow rates required a shorter elapsed time for the given volumetric restriction imposed by the inverted cup. The influence of this reduction in time is discussed later in this section. The error in Δt, related to the error in computer clock timing, is negligibly small in all cases.

The estimate of standard deviation found in the area of the receiver, A_r (see section titled ''Evaluation of $\langle U\rangle$'') was used as the estimate of the error δA_r, namely, $\delta A_r=0.0004\ m^2$ and $A_r=0.2136\ m^2$. The normalized error ($\delta A_r/A_r$) remained constant for jets of both widths. The error in the area of the jet, δA_j, was determined from conservative estimates of errors in the span B_N, and the width, w of the jet. The jet widths were measured carefully several times during the course of this investigation. The estimates of standard deviation of the measured values were determined and used as estimates of error δw. Table 1 lists the values of δw for the two jets. The span B_N was common for both jets; a conservative value of $\delta B_N=0.5$ mm has been used to determine δA_j in each case. Extreme combinations of B_N and w were used to compute the estimate of error δA_j. Table 1 also lists the estimates of the areas A_j and the corresponding error estimates δA_j.

The last term in the error propagation formula (Eq. (9)) relates to the error in the coefficient of linear regression used in the correlation of the VFS voltage E_p and the head of water column h_G in the reservoir G. The corresponding estimates of standard error were determined using the method described by Beck and Arnold [10], p. 43, for both coefficients: β_0 and β_1. The estimate of standard error were determined. The estimate of standard error in β_1 was used for $\delta\beta_1$; the values were: $\beta_1=25.22$ mm/volt and $\delta\beta_1=3.5719\times10^{-3}$ mm/volt.

Figure 2 presents the estimates of relative uncertainty in the measurements of $\langle U\rangle$ made in jets with $w=12.7$ mm and 25.4 mm using water and water-sugar mixture. A similar, and strong dependence on Re is evident for both water jets. The beneficial effect of using the more viscous water-sugar mixture over water is also observed for low Re cases. Around Re=1000, the relative uncertainty in $\langle U\rangle$ for a water jet is about twice the corresponding value for a water-sugar jet; this factor increases with decreasing Re. For

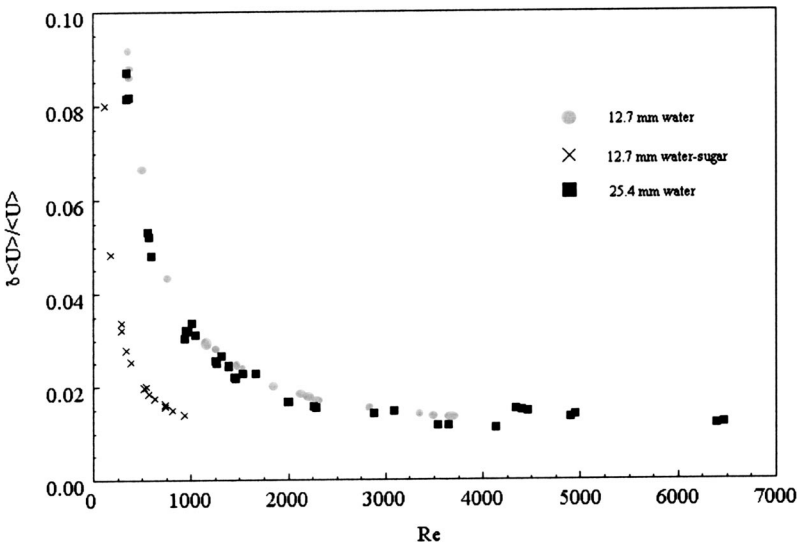

Fig. 2 The relative uncertainty in the measurements of $\langle U \rangle$ as a function of Re

a given Re, the high viscosity water-sugar mixture has to be run at a higher velocity $\langle U \rangle$ as compared with a water jet at the same Re. For a given jet width w and run time Δt, the higher velocity water-sugar jet results in a higher volume flow from the jet resulting in a higher voltage difference ΔE_p. This reduces the relative uncertainty in $\langle U \rangle$. In addition, the higher density of the water-sugar jet causes a higher hydrostatic pressure as compared with a water jet thus producing a favorable condition of reducing measurement uncertainty.

Figure 2 shows that the estimates of relative uncertainty in $\langle U \rangle$, with increasing Re, tend to assume an asymptotic value of about 1%; however, an increase to nominally 1.5% is observed at Re $>$4200. This is caused by the reduction in the run time Δt discussed earlier in this section. (This shows that the relative uncertainty at low Re could have been reduced by regulating the run time Δt.)

Regarding the uncertainty in the measurement of the velocity on the centerline of the jet, $\delta(U_0)/U_0$, it is noted that U_0 was measured using a laser Doppler velocimeter (LDV). This device, unlike other instruments, is not required to undergo calibration. However, in order to gain confidence that all elements of the LDV system were functioning as expected. The system was checked by measuring the linear velocity of a clear plastic wheel mounted on a speed regulated DC motor. The velocities reported by the LDV measuring system compared quite well with the velocities of the disk.

Hence, considering Eq. (9), the uncertainty in $\delta\langle U \rangle/\langle U \rangle$ is taken to represent the uncertainty in $\delta C_D/C_D$.

Results and Discussion

Laser Doppler velocimetery measurements along the centerline of the jet: $\overline{u}(x,0)$, as described by Ali [4] have been executed for $500 \leqslant \mathrm{Re} \leqslant 2900$. The experimental protocol for these measurements produced one time series of $u(x,y=0,t_k)$ values for each experiment at each x location and each sample time (t_k) for the LDV measurement. Hence, there are corresponding uncertainties in the $\overline{u}$, the $\langle U \rangle$, and the x locations for each data set. The uncertainties in the two velocities have been discussed in the previous section. The agreement between $\overline{u}(x,0)$ for the experimental and the potential flow cases is considered to be quite strong as shown in Fig. 3; the reported values are the best estimates of the results with a 95% confidence and with a nominal uncertainty of the order of 1%. The strong agreement shown in Fig. 3 between the experimental and the potential flow results does not extend to the C_D values as noted below.

Figure 4 presents the values of discharge coefficient, C_D, as a function of Re. The relative uncertainty in the determination of C_D has been estimated in the previous section to vary from 1% to nominally 9% for the lowest Re values with a confidence interval of 95%. At low values of Re ($<$800), C_D shows a strong Re dependence in which C_D increases as Re decreases. Given the results of the uncertainty analysis presented in the previous section, especially for Re$<$1000, it is important to consider the influence of uncertainty on the trend of C_D just described. For Re between 300 and 1000, the plot in Fig. 4 contains data from three independent jets. The uncertainties for water as the working fluid and for both widths were relatively large: 3%–9%. However, the uncertainty for the water-sugar jet was significantly lower 1.5%–2.5%, as shown in Fig. 2. In contrast, the C_D data (see Fig. 4) in the same range of Re exhibited similar values for jets of both liquids and both widths. In other words, even though the uncertainty estimates of C_D for the low Re data are relatively high, the trends shown by the C_D values for the three independent jet widths are in quite good agreement.

The observation that C_D depends strongly on Re for Re$<$800, can be made rational by noting that the boundary layer thickness, at the separation lip, will increase as the Re value is decreased. Since the fluid near the nozzle wall will have less inertia than that of the unsheared fluid, and since the physical extent of the former will be increased as the Reynolds number is decreased, the near wall fluid will be able to execute a curved path with a smaller radius of curvature as the Reynolds number is decreased. In this regard, it can be expected that the jet width at the vena-contracta will be larger for smaller Re values. This interpretation of the physics of the flow is compatible with the observed increase in the C_D values as the Re value is decreased below a nominal value of 800. By extension, this physical reasoning would suggest that the value of C_D would approach 0.611, the value of C_D for a slit jet flow of an inviscid fluid, in the limit as the Re value becomes large. This expectation was not, however, supported by the measurements. As shown in Fig. 4, C_D apparently achieves an asymptotic value of 0.687 for Re$\geqslant$2000 and for the $t_N/w=0.5$ nozzle configuration. The C_D values for $t_N/w=1.0$ configuration are larger (for Re$\geqslant$1500) and the limited Re range does not permit a corresponding limiting value to be confidently inferred, al-

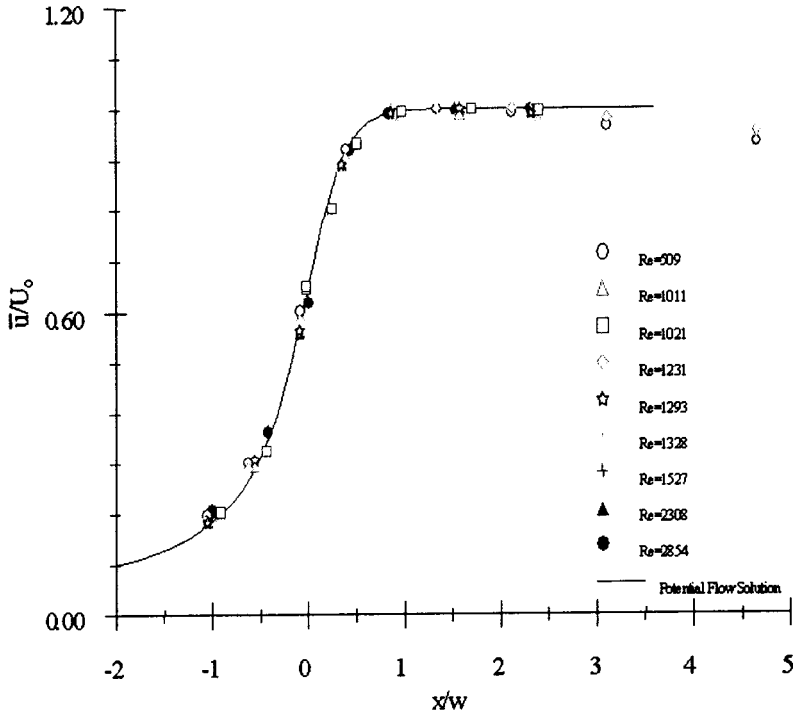

Fig. 3 Normalized mean velocity distribution along the centerline of the jet. The solid line represents the potential flow velocity distribution. The accuracy of the measured velocity is estimated to be within ±1%.

beit a value of 0.717 is suggested by the trend of the available data. This suggests that the contraction of the jet is greater for $t_N/w=0.5$ than in the case of $t_N/w=1$. The 0.687 value is about 12% larger than the 0.611 value predicted by the potential flow analysis.

Idelchik [11] quotes, without further attribution, a range of discharge coefficients: 0.598–0.609, for a thin slit-jet (t_N less than or equal to 0.03 w) that separates an upstream plenum from a downstream receiver. For the reasons stated above, the present authors consider the potential flow value: $C_D=0.611$, to be the minimum possible value for this geometric configuration. It is, therefore, inferred that: (i) the Idelchik values represent a bias error in the experimental procedure (unspecified) that was used to obtain them, or (ii) the orifice was not sharp edged.

The apparent asymptotic approach to 0.687 in Fig. 4 suggests the presence of a geometry-dependent effect on the C_D values.

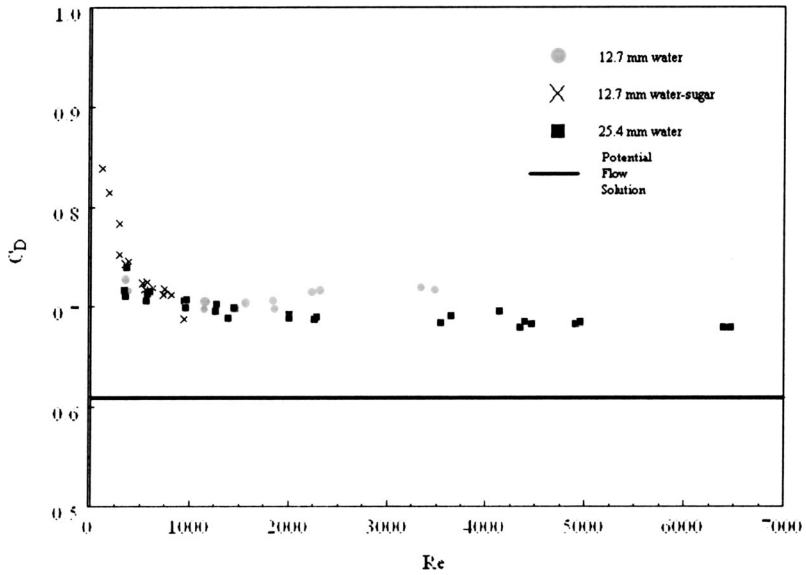

Fig. 4 Distribution of discharge coefficient C_D as a function of Re in jets with two different nozzle configurations: [$w, t_N/w, B_N/w$] [12.7 mm, 1, 21.7] and [25.4 mm, 0.5, 10.8]. Note that two different working liquids were used for the jet with $w=12.7$ mm. See Fig. 2 for the corresponding estimates of uncertainty in C_D. The solid line represents the potential flow solution for C_D.

Specifically, it is inferred that the values are influenced by the thickness, t_N, of the nozzle plate, and by the wedge angle α_N, for this relatively thick nozzle. See Fig. 1 for the t_N and α_N definitions. (This latter value is 60° in the present study and it is apparent that this angle will influence the C_D value as $\alpha_N \rightarrow 90$ deg.) Support for the inference of the (t_N/w) effect is provided by the C_D data in which two different slit-widths were used.

The influence of the nozzle-plate geometry on $\mathbf{V}(0,y \approx \pm w/2,z)$ for Re>1500 was suspected to be caused by an alteration of the entrainment path in the near-field of the jet. In the case of the relatively thicker nozzle plate $(t_N/w \approx 1)$, there will be more obstruction to the entrainment flow than in the case of the relatively narrower nozzle plate $(t_N/w \approx 0.5)$. Variations in the entrainment flow can alter the pressure field in the vicinity of the jet exit which, it is inferred, allows the relatively thicker nozzle plate flow to contract less at its vena-contracta as compared to the flow contraction associated with relatively thinner nozzle plate. The overlapping of the C_D values, for the two jets, below Re ≈1500 suggests that for these values of Re the viscous effects are dominant, and therefore, the near-field is less sensitive to the geometry of the nozzle. The present results suggest that the flow field for Re<1500 may be ''universal'' in nature, i.e., free from geometry-dependent effects. This inference has not been experimentally evaluated.

The inference, that t_N/w is the causal factor for the experimental C_D values to be larger than the potential flow value, is given support by the thickness constraint quoted by Idelchik [11]. Namely, the present experimental thickness values: 0.5w and 1.0w, are significantly larger than the largest acceptable value: 0.03w, given in that reference.

It is known from the previous studies, [4–7], that the submerged jet becomes unstable and develops symmetric (and spanwise) vortex motions for Re values greater than 250. Figure 4, however, shows a continuous decrease in the C_D values with increasing Re without a marked variation around Re≈250. It is therefore inferred that the formation of the vena-contracta is influenced only by the development of the boundary layers on the nozzle plates and not by the formation of vortices downstream of the exit plane.

Reference was made at the beginning of this section to the excellent agreement between the calculated and the measured (over a sixfold range of Re) values of $\overline{u}(x/w, y/w=0)/U_0$; see Fig. 3. The velocity field: $u(x,0,t)$, that is time-averaged to obtain these observed values, can be reliably described by the Euler ''s'' equation since the conditions of ''inviscid flow behavior'' and ''incompressible flow'' are clearly valid from the upper plenum to the vena-contracta. The third constraint: steady flow, that would be required for the derivation of the Bernoulli equation is not strictly valid for this flow condition given the presence of the vortex motions. The Bernoulli equation, for this flow, would be

$$p_k(x,0) + \rho \frac{\overline{u}^2}{2}(x,0) = p_k(\text{plenum}) \tag{10}$$

where $p_k = p + \rho g x$ is the ''kinetic pressure'' introduced by Potter and Foss [12] as an appropriate variable that combines the local static pressure and the gravitational body force effect in the differential momentum equation.

The LDV data of Ali [4] show that the velocity fluctuation $(\tilde{u})$ levels are nominally: $(\tilde{u})/U_o = 0.041$ at $x/w=1$. Hence, it is reasonable that the experimental data show qualitative agreement with the ''steady-state'' conditions of Eq. (10).

Considering the good agreement (shown in Fig. 3) between the calculated and the measured longitudinal velocity distribution over the Re range 500–2900, the strong dependence of C_D on Re over the same Re range shows that the influence of shear effects (development of boundary layers) on the nozzle plates is offset by some other physical effect. The Euler-n equation relates the centerline pressure, $p_k(x,y=0)$, to the radius of curvature, R, and the velocity, V, along a curved path ''n'' which is everywhere normal to the local streamlines and which extends from the atmosphere (1) to the jet centerline (2). This trajectory is shown schematically in Fig. 5. The centerline p_k distribution is given by

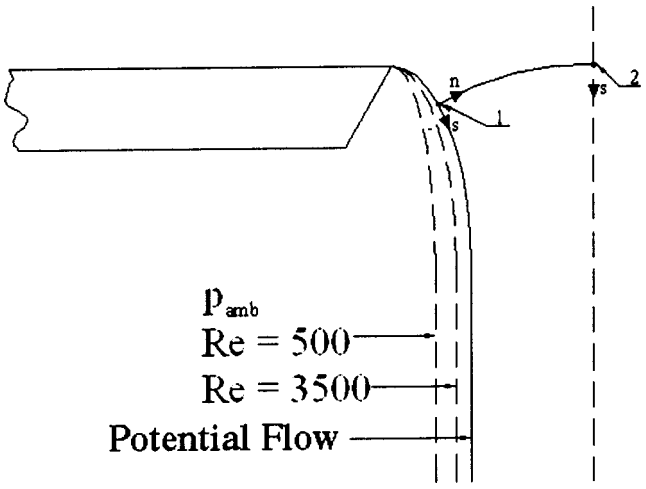

Fig. 5 Schematic representation of the influence of Re on the trajectory of the separating streamline. The curve 1–2 represents the path of integration normal to the streamline.

$$p_k(x,0) = p_{k\text{-amb}} + \int_1^2 \frac{\rho V^2}{R}\, dn \tag{11}$$

where $p_{k\text{-amb}}$ is the ambient pressure in the receiver. (See, for example, Potter and Foss [12], for the kinetic pressure as well as the Euler n equation development.) It has been argued above that the radius of curvature of the separating streamline (near $x=0$, $y=\pm w/2$) increases with increasing value of Re. Hence, the integration path 1–2 shown in Fig. 5 will also change with Re. Apparently, this change occurs such that the nondimensional pressure distribution along the centerline remains independent of Re. In other words, an adjustment in the curvature of the streamlines in the vicinity of the exit plane of the jet is believed to be responsible for the quantitative agreement of the viscous and the potential flow $p_k(x,y=0)$ distributions. Note that in this description $p_{k\text{-amb}}$ has been assumed to be constant along the curved path of the separating streamline. However, given the results of difference in the values of C_D for the two jets, and the fact that the asymptotic value of C_D is different from C_D $(t_N/w \approx 0)$, it is conjectured that p_k is smaller than the ambient value in the corner between the beveled surface of the nozzle plates and the separating streamlines. This will cause the jet to deflect outward from the centerline thus resulting in a larger value of C_D. The complete inference is, then, that a combination of the modified streamline trajectories and the reduced pressure near the separation point, are responsible for the increased C_D value. These effects would be difficult to experimentally assess. An accurate numerical simulation may be the most effective way to test this hypothesis.

Conclusions

The discharge coefficient, C_D, of a submerged two-dimensional slit-jet shows a strong Re dependence for Re<800. For higher values of Re and for the nozzle design: $t_N/w=0.5$, $\alpha_N=60$ deg, C_D achieves an asymptotic value of 0.687, which is nominally 12% higher than the potential flow value: 0.611. (The measurement uncertainty is ±1.5% for Re>2000 with a confidence interval of 95%). The experimental data also suggested an asymptotic value of $C_D=0.720$ for $t_N/w=1.0$ albeit the data are not sufficiently complete to fully test this inference. Hence, a geometric, as well as a Reynolds number, dependence is inferred for the slit-jet C_D values. The convergence of the C_D values for Re <1500 suggests the limited influence of the geometric parameter:

t_N/w, for low Re values. Conversely, it is conjectured that a geometric parameter: the shape of the downstream portion of the nozzle, influences the entrainment path of the fluid for Re >1500. This shape is inferred to alter the pressure field near the exit plane which, in turn, increases the discharge coefficient in response to these entrainment/pressure field effects.

Acknowledgments

This investigation was initially supported by the National Science Foundation through grant number MEA 8216946. Both authors acknowledge the subsequent support provided by the Michigan State University, E. Lansing, MI. The first author would also like to acknowledge the travel grant provided by the GIK Institute of Engineering Sciences & Technology, Topi, Pakistan, where he served as Visiting Associate Professor of Mechanical Engineering, during the preparation of this manuscript.

Nomenclature

$A,B,C,D,$
E,F,G,I = elements of the experimental facility (see Fig. 1)
A_j = area of slit-jet$=w\times B_N$
B_N = breadth of nozzle
C_D = discharge coefficient of the slit-jet (see Eqs. (1) and (3))
g = acceleration due to gravity
h = head of liquid column in the NH above the liquid level in the receiver G (see Fig. 1)
h_I = head of immersion depth in the volume flow sensor B (see Fig. 1)
h_G = head of liquid in the receiver G
H = distance between the walls of the channel-like plenum (see Fig. 1)
$\mathbf{i}$ = unit vector in the streamwise direction
n = outward direction normal to stream line (see Fig. 5)
p_k = kinetic pressure (see Eq. (11))
p_l = pressure in the inverted cup of the volume flow sensor B (see Fig. 1)
p_0 = kinetic pressure at vena-contracta where $\overline{u}=U_0$ (see Eq. (11))
R = radius of curvature of the separating streamline of the jet (see Eq. (11))
Re = Reynolds number based on w and $\langle U\rangle$
t_N = thickness of nozzle plate (see Fig. 1)
$\langle U\rangle$ = spatial/temporal average velocity of the jet at $x=0$ (see Eq. (2))
U_0 = $\overline{u}\,(x\approx x_m, y=0)$; $x_m\approx w$ for a viscous fluid, and $x_m\rightarrow\infty$ in the potential flow case
$\overline{u}$ = time mean of the longitudinal velocity $u(x,y,t)$
u' = fluctuating component of $u(x,y,t)$
V = magnitude of velocity
V_r = velocity sensed by the cup of the volume flow sensor B (see Fig. 1)
$\mathbf{V}$ = time mean velocity vector
w = slit width
x, y, z = streamwise, lateral, transverse coordinates

Greek Symbols

α_N = bevel angle (see Fig. 1)
β_0,β_1 = coefficients of linear regression (see Eq. (5))
υ = kinematic viscosity
ρ = density

References

[1] Blevins, R. D., 1984, *Applied Fluid Dynamics Handbook*, Van Nostrand Reinhold, New York.
[2] Birkhoff, G., and Zarantonello E. H., 1957, *Jets, Wake and Cavities*, Academic Press, New York.
[3] Vallentine, H. R., 1959, *Applied Hydrodynamics*, 2nd Ed., Butterworths Scientific Publications, London.
[4] Ali, S. K., 1991, "Instability Phenomena in a Two-Dimensional Slit-Jet Flow Field," Ph.D. dissertation, Michigan State University, East Lansing, MI.
[5] Beavers, G. S., and Wilson, T. A., 1970, "Vortex Growth in Jets," J. Fluid Mech., **44**, pp. 97–112.
[6] Clark, J. A., and Kit, L., 1980, "Shear Layer Transition and the Sharp-Edged Orifice," ASME J. Fluids Eng., **102**, pp. 219–225.
[7] Foss, J. F., and Korschelt, D., 1983, "Instabilities in the Slit-Jet Flow Field," J. Fluid Mech., **134**, pp. 79–86.
[8] Ali, S. K., and Foss, J. F., 1995, "A Computer Controlled, Finite Duration 'Steady,' Flow Facility," Exp. Fluids, **19**, pp. 250–254.
[9] Adrian, Ronald J., 1983, "Laser Velocimetry," *Fluid Mechanics Measurements*, Richard J. Goldstein, ed., Taylor and Francis, Philadelphia.
[10] Beck, J. V., and Arnold, K. J., 1977, *Parameter Estimation in Engineering and Science*, John Wiley and Sons, New York.
[11] Idelchik, I. E., 1994, *Handbook of Hydraulic Resistance*, 3rd Ed., CRC Press, Boca Raton, FL.
[12] Potter, M. C., and Foss, J. F., 1982, *Fluid Mechanics*, Great Lakes Press, Okemos, MI.